Pulsar Induced Axion Fields: A MOLE Implementation

Surbhi Dhiman and Miguel A. Dumett

May 4, 2026

Publication Number: CSRCR2026-04

Computational Science & Engineering Faculty and Students Research Articles

Database Powered by the Computational Science Research Center Computing Group & Visualization Lab

COMPUTATIONAL SCIENCE & ENGINEERING

SAN DIEGO STATE UNIVERSITY

Computational Science Research Center
College of Sciences
5500 Campanile Drive
San Diego, CA 92182-1245
(619) 594-3430

Pulsar Induced Axion Fields: A MOLE Implementation

Surbhi Dhiman* and Miguel A. Dumett †‡

May 4, 2026

Abstract

This investigation extends the Poddar and Mohanty's 2020 spherically symmetric one-dimensional axion field model to two dimensions by introducing an angular dependence through a Legendre polynomial modulation of the nucleon density, approximating the rotational oblateness of a pulsar. The resulting nonlinear elliptic Klein-Gordon equation is solved numerically using Newton's method with the Mimetic Operators Library Enhanced (MOLE). The solution demonstrates that breaking spherical symmetry produces a small but localized angular asymmetry in the axion field, with the field extending slightly further at the pole than at the equator, consistent with physical expectations.

1 Introduction

1.1 Background

One of the major problems in physics, known as the strong Charge-Parity (CP) problem, is a puzzle where the strong nuclear force mathematically allows for a fundamental asymmetry between matter and antimatter, yet

*Computational Science Master Program at San Diego State University (sdhiman1487@sdsu.edu).

†Editor: Jose E. Castillo

‡Computational Science Research Center at San Diego State University (mdumett@sdsu.edu).

experiments show this symmetry is preserved to extremely high precision, with no explanation in the Standard Model. We see this symmetry violation in the weak nuclear force, but not in the strong force. In 1977, Peccei and Quinn proposed a solution to this problem by introducing a new mechanism of nature that naturally explains why this symmetry is preserved [3, 4]. A consequence of this mechanism is an extremely light hypothetical particle called the axion.

Axions with certain properties turn out to be excellent dark matter candidates [6], which make up a majority of matter and gravitationally binds galaxies together.

Axions have never been directly detected, so scientists have been developing creative ways to search for them, ranging from laboratory experiments to astrophysical observations. One promising idea is to use pulsars which are rapidly rotating neutron stars [2]. They can be around 1.5 times the mass of the sun but are squeezed into a sphere smaller than the size of a city, with a radius on the order of 10 km. Pulsars have extremely compact densities, strong magnetic fields, and emit polarized radiation [7]. This intense environment is ideal for sustaining a non zero axion field inside the star which extends beyond the stars surface in an invisible halo also known as long range axion hair.

Axions can be very weakly coupled to photons [8] and produce an observable called birefringence [5] which occurs when the two components of light travel at different speeds, causing the plane of polarization to rotate as it travels through the axion field. If birefringence is observed in light emitted from pulsars, it could serve as a direct signature of the axion field.

In the Poddar and Mohanty's 2020 model [5], the axion field profile is solved by a static Klein-Gordon equation for a spherically symmetric, radial 1D case. The neutron star interior is treated as a constant density medium that induces an effective mass for the axion, while the exterior region falls off as a Yukawa tail. The interior and exterior solutions are matched at the stellar surface using continuity conditions. Poddar and Mohanty use this axion field to calculate the birefringence observable, but this study focuses on solving the 2D axion field as a nonlinear elliptic Klein-Gordon partial differential equation in two spatial dimensions.

1.2 Motivation

Neutron stars and pulsars are not perfectly spherical and thus are not accurately represented by a spherically symmetric model. The intense rotation of these stars causes a slight oblateness, which introduces a second degree of freedom. In the model, this is represented by including an angular dependence by adding a Legendre polynomial $P_2(\cos\theta)$ term in the equation for measuring the axion potential.

Another consideration in the Poddar and Mohanty's model is that the axion field equation is piecewise defined, constant inside the star and a continuous exponential fall outside it, leading to a sharp transition at the surface of the star. In this extended model, we introduce smoothness at the stellar interior to exterior transition by using a hyperbolic tangent tanh function instead of a step function for differentiability.

The Klein-Gordon equation describes how a relativistic scalar field evolves in spacetime under the influence of a potential. Since the system is described by this nonlinear PDE, there is no known closed form solution, and it must be solved numerically.

1.3 Objectives

The main computational objective of this effort is to solve the 2D nonlinear PDE for the dimensionless axion field $u(r, \theta)$. A converged solution should indicate the spatial structure and strength of the axion field both within the star and in the stellar exterior. This solution should also provide some insight into the effect of the angular deformation on the axion field structure, as well as, if the behavior changes across different mesh resolutions.

The physical outputs of the model should include the axion field contours as well as the difference between the radial profiles of the axion fields at the equator vs the pole of the star.

This implementation also tests the Mimetic Operators Library Enhanced (MOLE) [1] framework for implementing nonlinear PDEs.

2 Method

2.1 Formulation

2.1.1 Governing PDE

The governing equation in this MOLE implementation is a time-static, nonlinear Klein-Gordon equation of the form below where the Laplacian ∇^2 operator applies in spherical coordinates under axisymmetry. The right hand side of the equation represents the nonlinearity of the PDE, where the axion field potential is scaled by the square of the axion effective mass κ.

$$\nabla^2 u = \kappa \frac{\partial V}{\partial u}$$

This system is expressed in natural units where $G = c = \hbar = 1$, and so this PDE is dimensionless and scaled such that the radius of the star is at $r = 1$.

2.1.2 Derivation

The Poddar and Mohanty model starts with a 1D radial axion potential. The authors solve $\nabla^2 a(r) = \frac{\partial V}{\partial a}$, where a(r) represents the axion field equation and V represents the axion field energy potential. From [5, p. 28]:

$$V = -m_\pi^2 f_\pi^2 \left(\epsilon - \frac{\sigma_N n_N}{m_\pi^2 f_\pi^2}\right) \left|\cos\left(\frac{a}{2f_a}\right)\right|$$

In the 1D case, the value of the nucleon number density n_N is either constant in the interior of the star, or 0 in the exterior. In reality, neutron stars and pulsars can rotate so quickly that the stars bulge more towards the equator, thus adjusting the n_N value. To form a 2D case, we introduce the second Legendre polynomial, dependent on θ, as a term to break spherical symmetry and describe an axisymmetric case. We also introduce a smoothening function term that smooths the transition between interior and exterior at $r = R$ surface of the star to allow for differentiability:

$$n_N(r,\theta) = n_0 \cdot \frac{1}{2}\left[1 - \tanh\left(\frac{r-R}{\delta_1}\right)\right] \cdot \left[1 + \beta\frac{1}{2}\left(3\cos^2(\theta) - 1\right)\right]$$

Note that modeling the rotation via an angular modulation of nucleon density is a leading order approximation meant to mimic rotational oblateness without solving an explicitly deformed stellar surface.

In the 1D axion potential, the absolute value $\left|\cos(\frac{a}{2f_a})\right|$ term leads to discontinuity in the model. Introducing a numerical regularization parameter δ_2 to ensure differentiability with approximation $|x| \approx \sqrt{x^2+\delta_2}$ for small δ_2. Substitution in the 2D number density gets the new effective potential:

$$V = -m_\pi^2 f_\pi^2 \left(\epsilon - \frac{\sigma_N}{m_\pi^2 f_\pi^2} \cdot n_N(r,\theta)\right) \sqrt{\cos^2\left(\frac{a(r,\theta)}{2f_a}\right) + \delta_2^2}$$

Rescaling parameters help stabilize the PDE to solve. A dimensionless of the model also clarifies which computational parameters and physical ratios are important in the model.

To obtain the non-dimensionalization, let:

- $u(r,\theta) \equiv \frac{a(r,\theta)}{2f_a} \longrightarrow \nabla^2 u = \frac{1}{4f_a}\frac{\partial V}{\partial u}$
- $\overline{r} \equiv \frac{r}{R}$
- $\overline{n}_N \equiv \frac{n_N}{n_0} \longrightarrow \overline{n}_N(\overline{r},\theta) = \frac{1}{2}\left[1 - \tanh\left(\frac{\overline{r}-1}{\delta_1}\right)\right]\left[1 + \beta\frac{1}{2}\left(3\cos^2(\theta) - 1\right)\right]$
- $\overline{V} \equiv \frac{V(\overline{u};\overline{n}_N(\overline{r},\theta))}{m_\pi^2 f_\pi^2} \longrightarrow \overline{V} = -\left(\epsilon - \frac{\sigma_N n_0}{m_\pi^2 f_\pi^2} \cdot \overline{n}_N(\overline{r},\theta)\right)\sqrt{\cos^2(\overline{u}) + \delta_2^2}$

Applying the substitutions, the 2D PDE to solve becomes:

$$\nabla^2 \overline{u}(\overline{r},\theta) = \kappa \frac{\partial \overline{V}}{\partial u}$$

where $\kappa = \frac{R^2 m_\pi^2 f_\pi^2}{4f_a^2}$ is dimensionless.

For the sake of clarity, remove the bars over the non-dimensional variables of the computational model, so that:

$$\overline{V} \to V \qquad ,\overline{r} \to r, \qquad \overline{u} \to u, \qquad \overline{n} \to n, \qquad \overline{\nabla} \to \nabla.$$

Let

$$\chi(n_N; r, \theta) = \epsilon - \frac{\sigma_N n_0}{m_\pi^2 f_\pi^2} \cdot n_N(r,\theta)$$

then

$$V = -\chi\sqrt{\cos^2(u) + \delta_2^2},$$

and the first derivative of the potential becomes:

$$\frac{\partial V}{\partial u} = \chi \cdot \frac{\sin(u)\cos(u)}{\sqrt{\cos^2(u) + \delta_2^2}}$$

Plugging this back into the dimensionless Klein-Gordon equation

$$\nabla^2 u(r,\theta) = \kappa \cdot \chi(n_N; r, \theta) \cdot \frac{\sin(u)\cos(u)}{\sqrt{\cos^2(u) + \delta_2^2}}$$

or equivalently,

$$\nabla^2 u(r,\theta) = \kappa \cdot [\epsilon - \chi_0 \cdot n_N(r,\theta)] \cdot \frac{\sin(u)\cos(u)}{\sqrt{\cos^2(u) + \delta_2^2}}, \tag{1}$$

where:

$$\kappa = \frac{R^2 m_\pi^2 f_\pi^2}{4 f_a^2}$$

$$\chi_0 = \frac{\sigma_N n_0}{m_\pi^2 f_\pi^2}$$

$$\chi(n_N; r, \theta) = \epsilon - \chi_0 \cdot n_N(r,\theta)$$

$$n_N(r,\theta) = \frac{1}{2}\left[1 - \tanh\left(\frac{r-1}{\delta_1}\right)\right]\left[1 + \beta\frac{1}{2}\left(3\cos^2(\theta) - 1\right)\right]$$

$$\nabla^2 u(r,\theta) = \frac{1}{r^2}\frac{\partial}{\partial r}\left(r^2\frac{\partial u}{\partial r}\right) + \frac{1}{r^2\sin\theta}\frac{\partial}{\partial\theta}\left(\sin\theta\,\frac{\partial u}{\partial\theta}\right).$$

2.1.3 Parameters

There are several physical variables and computational parameters applied in this PDE that are described in the following table.

Parameter	Meaning	Value
m_π	pion mass	$1.35 \cdot 10^8$ eV
f_π	pion decay constant	$9.2 \cdot 10^7$ eV
f_a	axion decay constant	10^{22} eV
σ_N	pion-nucleon sigma term	$5.9 \cdot 10^7$ eV
n_0	constant nucleon number density	10^{25}eV^3
R_{star}	radius of star	1
β	quadrupolar deformation measure	0.1
ϵ	strength of vacuum axion potential	0.01
δ_1	sharpness of transition at r=R	10^{-2}
δ_2	sharpness of abs value approximation	10^{-3}
κ	scales the square of axion effective mass	$3.86 \cdot 10^{-13}$
χ_0	scales nucleon density	3.82

2.1.4 Domain

For the radial domain, let r be the variable, $R = 1$ for radius of the star in dimensionless rescaled units, and $R_{max} \approx 20 \gg R$ is a truncated exterior of the domain that is large enough for the axion field to decay to 0. Hence,

- Stellar interior: $0 \leq r \leq R$
- Stellar exterior: $R < r < R_{max} \to \infty$

For the angular domain θ, assume equatorial symmetry. So, the total computational domain becomes:

$$(r, \theta) \in [0, 20] \times \left[0, \frac{\pi}{2}\right]$$

2.1.5 Boundary Conditions

- Regularity at the center of the star enforces homogeneous Neumann BC:

$$r = 0 \to \frac{\partial u}{\partial r}(0, \theta) = 0$$

- Axion field potential falling to 0 in the vacuum of space enforces homogeneous Dirichlet condition for far field vacuum:

$$r = R_{max} \rightarrow u(20, \theta) = 0$$

- Periodic boundary conditions are enforced in the θ direction for the numerical implementation. Note that the physical setup assumes symmetry about $\theta = 0$ and $\theta = \frac{\pi}{2}$.

2.1.6 Initial Condition

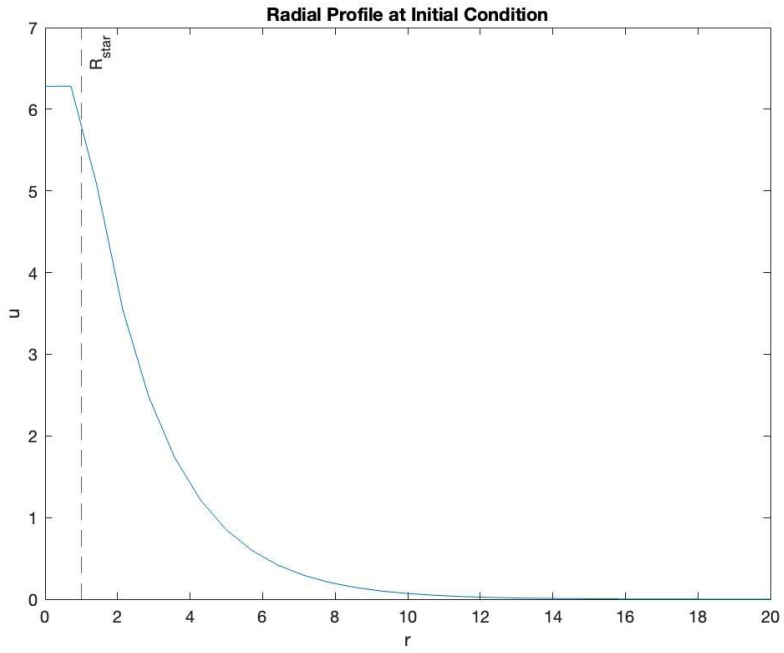

Figure 1: The radial profile of the initial condition. Note that the piecewise transition does not appear sharp at $r = R_{\text{star}} = 1$ due to a lower initial resolution of the grid, as the values at r=1 are interpolated by stellar interior and exterior points.

Since the basin of convergence is unknown, the complete algorithm calculates the solution across increasingly higher resolution values where the initial

condition for the $i+1$ iteration is the solution of the i^{th} iteration. The initial condition for the first iteration generally follows the radial piecewise solution as solved in the Poddar and Mohanty's model [5].

$$\begin{aligned} u(r,\theta) &= 2\pi, && r < R_{\text{star}} \\ u(r,\theta) &= 2\pi e^{-\frac{1}{2}(r-R_{\text{star}})}, && r > R_{\text{star}} \end{aligned}$$

2.2 Implementation

2.2.1 Weighted Laplacian for 2D Spherical Coordinates

MOLE naturally works with rectangular computational grids in 2D. By introducing polar coordinates one can transform the problem given in an angular domain to a rectangular one. Of course, this complicates the expressions for the Laplacian, the gradient, and the divergence, but the advantage of doing this is the simplicity of the computational domain.

The input data and outcomes values of the mimetic operators on the staggered grid are defined at cell centers, or cell face centers. For example, the divergence operator calculates values in the centers of the grid cells and the gradient operator translates the values back into the centers of the cell faces. Since the problem is defined in spherical coordinates under axisymmetry, spatial weights are applied to the divergence and gradient operators such that the Laplacian operates from centers to centers.

The polar Laplacian is obtained from the Cartesian Laplacian applying the polar transformation and is given by:

$$\nabla^2 u(r,\theta) = \frac{1}{r^2}\frac{\partial}{\partial r}\left(r^2\frac{\partial u}{\partial r}\right) + \frac{1}{r^2\sin\theta}\frac{\partial}{\partial\theta}\left(\sin\theta\frac{\partial u}{\partial\theta}\right)$$

Multiplying the right-hand side and the left-hand side of the PDE (1) by the factor of $r^2\sin\theta$ avoids dividing by 0 errors when $r = 0$. Then the polar Laplacian left-hand side becomes

$$r^2\sin\theta\,\nabla^2 u(r,\theta) = \sin\theta\frac{\partial}{\partial r}\left(r^2\frac{\partial u}{\partial r}\right) + \frac{\partial}{\partial\theta}\left(\sin\theta\frac{\partial u}{\partial\theta}\right)$$

Let G_r, D_r, G_{th}, D_{th} be the gradient and divergence matrix operators as defined in rectangular coordinates. Then, let

$$S_{th} = \begin{bmatrix} \sin\theta_{c,1} & & \\ & \ddots & \\ & & \sin\theta_{c,end} \end{bmatrix}$$

$$R_r = D_r \cdot \begin{bmatrix} r_{f,1}^2 & & \\ & \ddots & \\ & & r_{f,end}^2 \end{bmatrix} \cdot G_r$$

$$R_{th} = D_{th} \cdot \begin{bmatrix} \sin\theta_{f,1} & & \\ & \ddots & \\ & & \sin\theta_{f,end} \end{bmatrix} \cdot G_{th}$$

where S_{th} operates on the θ centers, R_r operates on the r faces, and R_{th} operates on the θ faces. The curvilinear Laplacian operator is then defined as:

$$L = S_{th} \otimes R_r + R_{th} \otimes \mathbb{I}$$

2.2.2 Nonlinear Terms

After scaling the RHS of (1) by the factor $r^2 \sin\theta$, the nonlinear term becomes:

$$\text{RHS} = r^2 \sin\theta \cdot \kappa \cdot [\epsilon - \chi_0 \cdot n_N(r,\theta)] \cdot \frac{\sin(u)\cos(u)}{\sqrt{\cos^2(u) + \delta_2^2}}$$

In the MOLE implementation this looks like:

$$\text{RHS} = \overrightarrow{W} \cdot g(\overrightarrow{u})$$

where

$$\overrightarrow{W} = \kappa \cdot \overrightarrow{r^2} \cdot \sin \overrightarrow{\theta} \cdot \overrightarrow{\chi}$$

$$\overrightarrow{P_2} = 0.5 \cdot \left(3 \cos^2 \overrightarrow{\theta} - 1\right)$$

$$\overrightarrow{n_N} = 0.5 \cdot \left(1 - \left(\tanh \frac{\overrightarrow{r} - R_{\text{star}}}{\delta_1}\right)\right) \cdot \left(1 + \beta \overrightarrow{P_2}\right)$$

$$\overrightarrow{\chi} = \epsilon - \chi_0 \cdot \overrightarrow{n_N}$$

$$g\left(\overrightarrow{u}\right) = \frac{\sin(\overrightarrow{u}) \cos(\overrightarrow{u})}{\sqrt{\cos^2(\overrightarrow{u}) + \delta_2^2}}$$

Note that the $\cdot$ between vectors denotes the Hadamard product on the computational grid.

2.3 Algorithm

2.3.1 Outer Loop: Mesh Refinement

For each resolution level m in $[27, 31, 35]$:

Step 1: Build the grid by computing d_r and $d_t h$ from domain limits and resolution, construct radial centers r_c, faces r_f, angular centers θ_c, faces θ_f, and define the 2D mesh grid $[TH, R]$.

Step 2: Construct the initial condition for the first iteration, use the analytic piecewise profile described in section 2.1.6. For subsequent iterations, interpolate previously converged solution U from the coarser grid to a finer grid resolution using spline interpolation, filling NaNs with 0, and enforcing homogeneous Dirichlet BC at r=20.

Step 3: Solve for current resolution by passing the resolution value, the initial condition, and domain limit to the solve_axions function. This calculates the solution on the new grid resolution.

2.3.2 Inner Function: solve_axions with Newton's Method

Step 4: Build operators for the divergence and gradient and combine to calculate the Laplacian operator as described in section 2.2.1.

Step 5: Construct RHS for the PDE as described in section 2.2.2.

Step 6: Apply weighted penalty by modifying the Laplacian $L_{\text{mod}} = L + \lambda \cdot \text{diag}(\text{mask})$ on the stellar interior nodes to preserve the constant axion field value within the star. Here, $\lambda = 1e5$ and the mask is only applied to nodes where $r \leq R_{\text{star}}$. The residual is also modified by adding a term F_{mod} that similarly adds stability to the stellar interior nodes. Note that this drives the solution to be consistent with the constant-field approximation in [5], rather than solving for the full interior dynamics.

Step 7: Newton iteration is repeated for up to max_iter=1500 iterations. Within each iteration:

- Compute the residual $F = L_{\text{mod}}\hat{A}U - W\hat{A}g(U) - F_{\text{mod}}$
- Compute the Jacobian $J = L_{\text{mod}} - \text{diag}(W \cdot g'(U))$ where $g'(U)$ is the first derivative of $g(U)$.
- Apply boundary conditions via addScalarBC2D
- Solve the linear system $dU = J^{-1} \cdot (-F)$
- Update the solution $U = U + \alpha \cdot dU$ where $\alpha = 0.01$ is the dampening parameter to aid with convergence.
- Check for convergence

Step 8: Reshape and return the solution U and grid values to the outer loop for plotting.

2.3.3 After converge

Step 9: Diagnostics and plotting for the solution values. Output plots include the radial profiles at the pole and the equator as well as a contour plot of the final solution $U(r, \theta)$.

3 Results

The final solution generally follows the shape of the initial condition, due in part to the interior penalty condition applied to the Laplacian. At $\theta = 0$, the nucleon density n_N is larger than at $\theta = \frac{\pi}{2}$, and so the axion field is pushed out slightly further at $\theta = 0$ than $\theta = \frac{\pi}{2}$, however the axion field quickly falls across all θ.

With the parameters in the current setup, the errors fall quickly at first and then slow down, hitting the max_iter value for each grid resolution with a low tolerance of $1e-3$, and then only stagnating with a damping parameter for the coarse resolution values, for $m \leq 39$. This damping parameter helps the solution stabilize around the tolerance, but likely suppresses convergence to the true solution in Newton's method. Although the solution did not fully converge for all resolutions, it is stabilized enough to capture the overall trends.

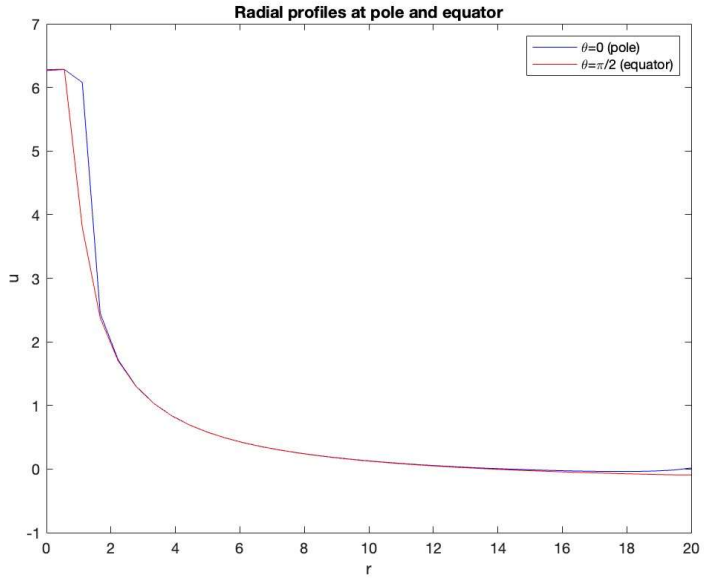

(a) Radial Profiles

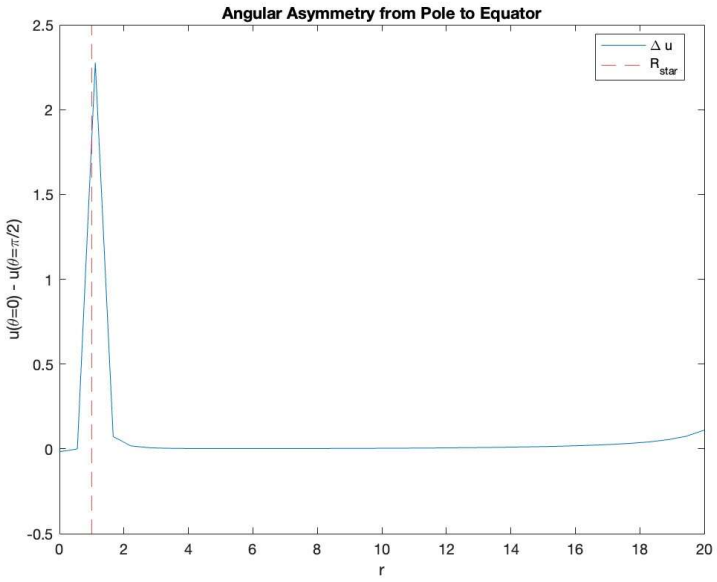

(b) Angular Difference

Figure 2: Radial profiles of the final solution at the pole and the equator and the behavior of the angular asymmetry along the radial axis.

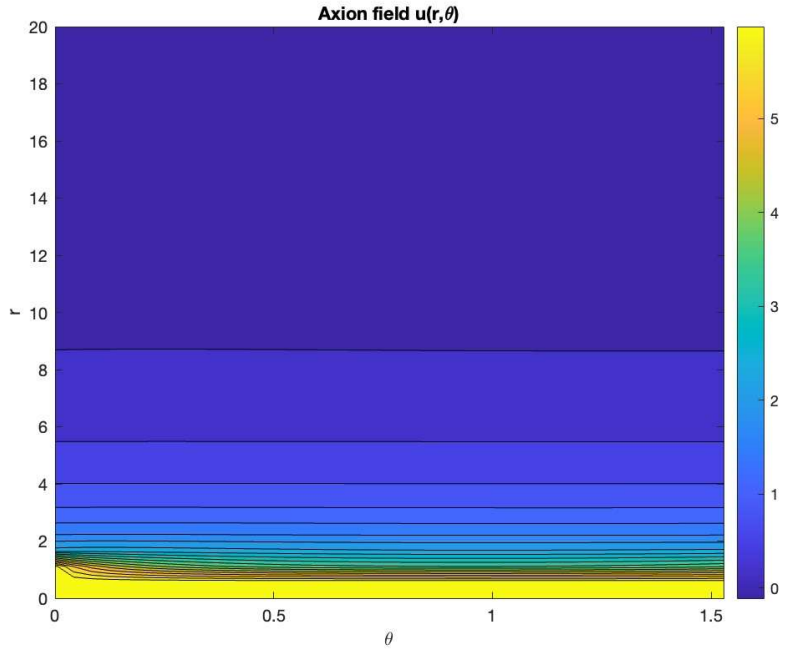

(a) Full field

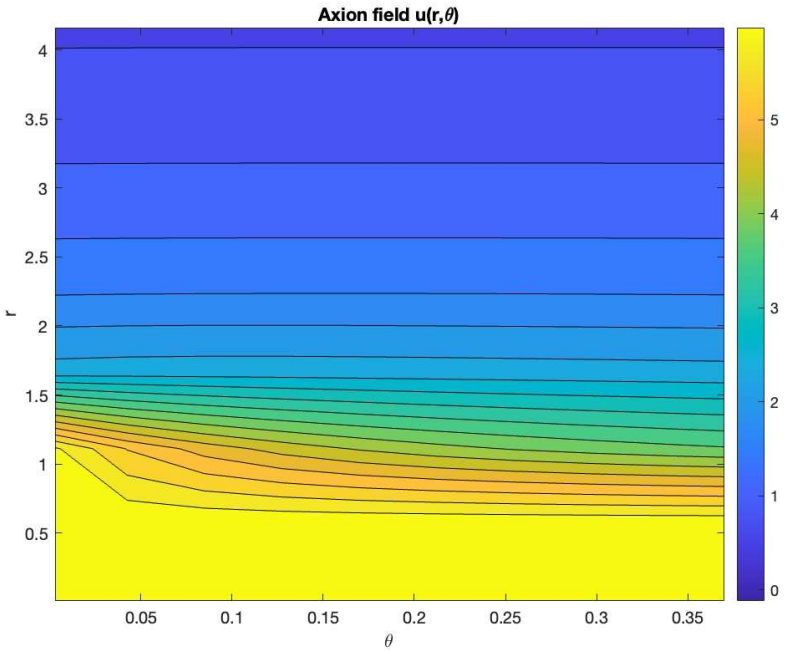

(b) Zoomed region

Figure 3: Axion field profile and zoomed-in structure near the stellar surface and near $\theta = 0$.

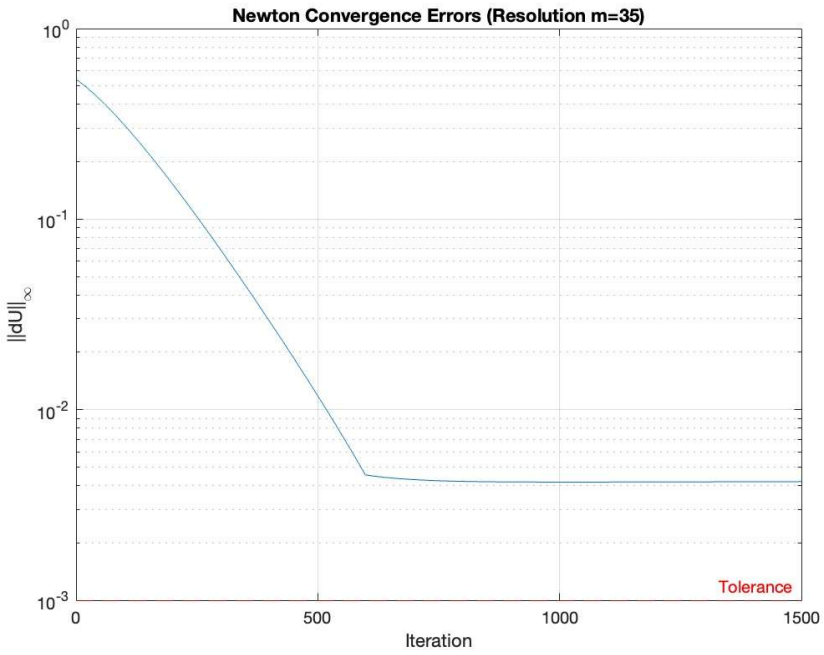

Figure 4: Convergence rate across the iterations of Newton's method for the final solution

4 Discussion

The final solution aligns with the physical expectation. Breaking the spherical symmetry does indeed alter the shape of the axion field around the star, however, the effect is quite localized and falls quickly to the symmetric case as θ increases from 0 to $\frac{\pi}{2}$. This may be due to choices of some of the computational parameters or an effect of the extension from 1D to 2D. For example, the quadrupolar deformation parameter β may be small or solutions for higher resolution grids diverge, limiting how well the angular structure is resolved.

Although this model extends the spherically symmetric radial case in the Poddar and Mohanty model, there are still several assumptions and approximations in this system. This model adjusts the nucleon number density in the axion field potential to model oblateness to only a first-order approximation, and does not fully represent a deformed stellar surface. The model also

generally assumes a constant nucleon density throughout the star, which does not take into account the radial structure predicted by realistic neutron star equations of state. Additionally, this calculation is performed in flat spacetime, ignoring general relativistic curvature effects due to the stars strong gravitational field.

5 Conclusion

In conclusion, we used Newton's method applied in MOLE to solve for a 2D nonlinear Klein-Gordon equation that computes the shape and strength of an axion field around a neutron star. As compared to the 1D case, we did see that there is a slight change in the axion field due to breaking the spherical symmetry.

This model only breaks the assumption of spherical symmetry to a first-order approximation and would require several very complex extensions to model a fully realistic neutron star equation of state in 4D spacetime, some of which are discussed in section 4.

Despite these limitations, this study is one step closer to evaluating whether neutron stars may indeed be used as a probe for axion discovery.

References

[1] Johnny Corbino, Miguel A. Dumett, and Jose E. Castillo. MOLE: Mimetic Operators Library Enhanced. *Journal of Open Source Software*, 9(99):6288, July 2024.

[2] Anson Hook and Junwu Huang. Probing axions with neutron star inspirals and other stellar processes. *Journal of High Energy Physics*, 2018(6), 2018.

[3] R. D. Peccei and Helen R. Quinn. Constraints imposed by CP conservation in the presence of pseudoparticles. *Phys. Rev., D*, 16(6):1791–1797, September 1977.

[4] R. D. Peccei and Helen R. Quinn. CP conservation in the presence of pseudoparticles. *Physical Review Letters*, 38(25):1440–1443, June 1977.

[5] Tathagata Poddar and Subhendra Mohanty. Probing the angle of birefringence due to long range axion hair from pulsars. *Physical Review D*, 102(8):083029, 2020.

[6] John Preskill, Mark B. Wise, and Frank Wilczek. Cosmology of the invisible axion. *Physics Letters B*, 120(1-3):127–132, January 1983.

[7] L. M. Shier and F. C. Michel. Modeling of pulsar polarization properties. *International Astronomical Union Colloquium*, 128:378â383, 1992.

[8] Günter Sigl and Pranjal Trivedi. Axion-like Dark Matter Constraints from CMB Birefringence. *arXiv e-prints*, page arXiv:1811.07873, November 2018.